Chemosphere 364 (2024) 143233

Contents lists available at ScienceDirect

Chemosphere

journal homepage: www.elsevier.com/locate/chemosphere

Cm(III) speciation in the presence of citrate from neutral to hyperalkaline conditions and the effect of calcium

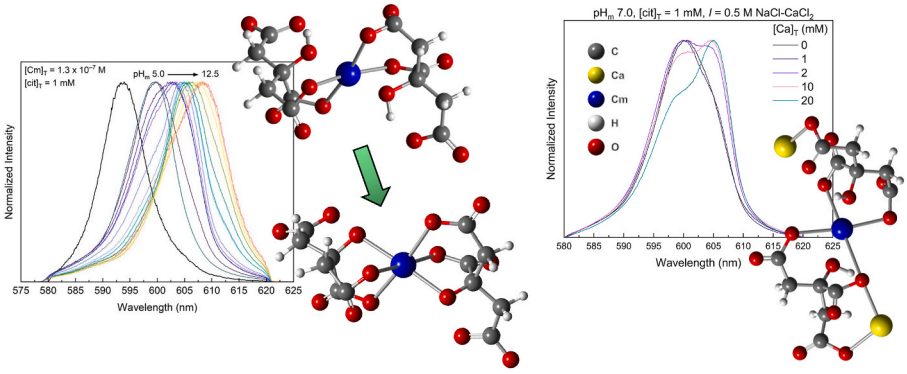
Matthew B. Comins [a,*], Chengming Shang [b,1], Robert Polly [b], Andrej Skerencak-Frech [b], Marcus Altmaier [b], Amy E. Hixon [a], Xavier Gaona [b,**]

[a] Department of Civil & Environmental Engineering & Earth Sciences, University of Notre Dame, 301 Stinson-Remick, Notre Dame, IN, 46556, USA
[b] Karlsruhe Institute of Technology, Institute for Nuclear Waste Disposal, P.O. Box 3640, Karlsruhe, 76021, Germany

HIGHLIGHTS

- Deconvolution of Cm-citrate TRLFS spectra from pH 5.0–12.5 resulted in 3 components.
- DFT supports stepwise deprotonation and coordination of the citrate alcohol group.
- Slope analysis revealed a linear slope = 1 for fraction species versus pH.
- Ternary Ca-Cm-citrate complexes are reported for the first time.

GRAPHICAL ABSTRACT



ARTICLE INFO

Handling Editor: Milena Horvat

Original content: Curium citrate TRLFS, PARAFAC, DFT (Original data)

Keywords:
Curium
Citrate
Calcium
TRLFS
PARAFAC
DFT

ABSTRACT

We investigated the binary Cm-citrate system using time-resolved laser fluorescence spectroscopy (TRLFS), parallel factor analysis (PARAFAC), and quantum chemical calculations. Evidence collectively suggests the stepwise coordination and deprotonation of citrate alcohol groups in Cm-cit complexes with two bound citrate moieties upon increasing pH, which is supported by a bathochromic shift in emission spectra, an observed increase in lifetime measurements, and lower energy minima for citrate alcohol involvement versus hydrolysis of the Cm-citrate species. Our PARAFAC results agree with a 3-component model for the Cm-citrate system and offer pure component decompositions, yielding fraction species across the studied pH range that have a correlated slope = 1 as a function of pH. For the first time, evidence of ternary Ca-Cm-citrate complexes was revealed by TRLFS with increasing calcium concentration at fixed pH_m. The formation of these ternary complexes was substantiated with density functional theory (DFT) calculations on simple model systems of the complexes. Shared citrate carboxylate groups between calcium and curium were proposed for all three ternary Ca-Cm-cit complexes based on DFT-determined Ca–O and Cm–O distances. Moreover, we found that the ternary

* Corresponding author.
** Corresponding author.
E-mail addresses: mbcomins@gmail.com, mcomins@nd.edu (M.B. Comins), colombe.chengming.shang@gmail.com (C. Shang), polly@kit.edu (R. Polly), andrej.skerencak@kit.edu (A. Skerencak-Frech), marcus.altmaier@kit.edu (M. Altmaier), ahixon@nd.edu (A.E. Hixon), xavier.gaona@kit.edu (X. Gaona).
[1] Current address:China Institute of Atomic Energy, Department of Radiochemistry, P.O. Box 2751, Beijing, 110111, China.

https://doi.org/10.1016/j.chemosphere.2024.143233
Received 8 July 2024; Received in revised form 29 August 2024; Accepted 30 August 2024
Available online 31 August 2024
0045-6535/© 2024 The Authors. Published by Elsevier Ltd. This is an open access article under the CC BY license (http://creativecommons.org/licenses/by/4.0/).

Ternary complexes
Coordination

complex with both alcohol groups deprotonated is most stable when it shares both two carboxylate and two alcohol groups between Ca and Cm. The presence of shared functional groups highlights the enhanced stability of these ternary complexes. Additional work is warranted to further constrain the stoichiometry, stability constants and dependence on ionic strength of these complexes for purposes of thermodynamic modeling of repository settings.

1. Introduction

Understanding actinide (An) mobility in underground repositories for nuclear waste is integral for safely disposing radiotoxic elements and limiting their mobilization into the biosphere to within acceptable dose rates. After repository closure, redox conditions are expected to become highly reducing mostly due to anoxic corrosion of steel and iron components (Schramke et al., 2020). In cementitious environments, as those considered in many repository concepts for low and intermediate level waste (L/ILW), hyperalkaline conditions ($10 \leq pH_m \leq 13.5$) and moderate calcium concentrations (10^{-3} M $\leq$ [Ca] $\leq$ 0.02 M) will dominate the pore water composition (Hicks et al., 2008; Bube et al., 2013). In the case of the Waste Isolation Pilot Plant (WIPP), alkaline conditions are expected to develop after interaction with MgO, producing a pH_m of approximately 9 (United States Department of Energy, 2014). In these reducing systems, actinides are predominantly expected in the oxidation states +III and +IV. An(IV) are characterized by low solubility and high sorption over a broad range of pH conditions, whereas An(III) show comparatively higher solubilities in weakly alkaline pH conditions, but become largely insoluble in the hyperalkaline pH regime (Guillaumont et al., 2003; Altmaier et al., 2019; Grenthe et al., 2020). The presence of organic ligands may lead to the formation of stable complexes with these radionuclides, eventually promoting their mobilization into the biosphere.

Citric acid ($C_6H_8O_7$), henceforth cit, is a tricarboxylic acid present in transuranic waste due to its use as a key decontaminant in the nuclear industry, and is applied as an additive in the cement industry to control setting and hardening of cementitious materials (Möschner et al., 2009; Kusbiantoro et al., 2013; Guidone et al., 2024). With four functional groups (up to 3 of which are able to coordinate with a metal ion), cit is known to form strong complexes with actinide ions. In the absence of metal ions, the hydroxyl (used interchangeably with alcohol) group on citrate does not deprotonate until pH > 14 (Silva et al., 2009a). However, the pKa for the citrate alcohol group is substantially lowered in the presence of metal ions (M = Ni(II), Fe(II), Fe(III), Al(III), Ga(III), Ln(III)), (Strouse, 1977; Hedwig et al., 1980; Baker et al., 1983; Öhman, 1988; Kieboom et al., 1977; Chunbo et al., 1995; Silva et al., 2009b; Motekaitis and Martell, 1984; Clausén et al., 2005; Jackson and du Toit, 1991) and is likewise expected to be so for trivalent actinide ions. For Ln(III) systems specifically, alcohol group involvement was found to occur at pH 7.4 (Chunbo et al., 1995). The deprotonation of the alcohol proton is written as "H_{-1}cit" in the present work. Understanding the coordination and deprotonation of the citrate alcohol group in actinide-citrate complexes is needed for proper determination of An-cit stability constants and accurate thermodynamic modeling of the An-cit system, but is made challenging by the chemically identical nature of hydrolysis versus deprotonation of the alcohol group.

Numerous studies are available regarding the complexation of trivalent actinides with citrate. An overwhelming majority of these studies, however, are confined to the acidic pH region, where the stoichiometry and thermodynamic data of citrate complexes are more easily and satisfactorily defined. The Nuclear Energy Agency Thermochemical Database (NEA-TDB) Project compiled and critically reviewed literature concerning An(III)-cit speciation (with An = Am and Pu), but only four complexes (mostly relevant in acidic conditions) were finally selected: $Am(Hcit)^+$, $Am(Hcit)_2^-$, Am(cit)(aq), and $Am(cit)_2^{3-}$ (Hummel et al., 2005). Fewer studies have investigated the neutral to alkaline conditions that are relevant to nuclear waste disposal (Moutte and Guillaumont, 1969; Bouhlassa and Guillaumont, 1984; Eberle and Moattar, 1972; Hummel, 1993; Aoyagi et al., 2018). Fewer among these have identified the stoichiometry and derived stability constants for ternary An(III)–OH–cit complexes, (Moutte and Guillaumont, 1969; Bouhlassa and Guillaumont, 1984; Eberle and Moattar, 1972) but these studies were either not included in the NEA review or not considered reliable enough for selection of thermodynamic data (Hummel et al., 2005). A detailed summary of the main thermodynamic studies available in the literature for the system An(III)-cit is provided in the Supporting Information. Table S1 provides a compilation of the complexation constants used in this work for scoping geochemical calculations involving the An(III)-cit system.

In the presence of Ca, above pH_m 5, the formation of the stable aqueous complex $Ca(cit)^-$ and solid phase $Ca_3(cit)_2{\cdot}4H_2O$(cr) are expected to limit the availability of this ligand for the complexation with radionuclides (Hummel et al., 2005). Under equimolar conditions of Ca and Cm, Cm would clearly outcompete Ca for citrate. However, the degree to which calcium will outcompete curium under higher Ca concentrations and neutral to alkaline conditions as those expected in specific repository systems, and the formation of possible ternary Ca-Cm-cit complexes, are principal foci of this study.

In this work, we investigated the interactions between Cm(III) (an Am(III) analog with favorable fluorescing properties) and citrate in the presence and absence of calcium. A combined approach using time-resolved laser fluorescence spectroscopy (TRLFS) and theoretical calculations is applied, with the aim of characterizing the chemical model, *i.e.*, subset of chemical reactions controlling the binary Cm(III)-cit and ternary Ca–Cm(III)-cit systems, in the alkaline to hyperalkaline conditions of relevance in the context of repositories for nuclear waste.

2. Experimental

2.1. Materials

Samples were prepared and stored in an anoxic, Ar-circulating glove box ($T = 22 \pm 2$ °C, $O_2 < 1$ ppm). Milli-Q (Millipore, 18.2 MΩ cm at 25 °C) ultrapure water was purged with argon gas prior to use in all solutions. Citrate solutions were prepared with trisodium citrate ($Na_3C_6H_5O_7{\cdot}2H_2O$(s); Sigma Aldrich, 99–101%) and pH was adjusted using NaOH (Titripur®) and HCl (Titrisol®). $CaCl_2{\cdot}2H_2O$(s) (Sigma Aldrich, 99–102%) was used in calcium-bearing samples. Ionic strength was adjusted to $I = 0.5$ M using NaCl (Sigma Aldrich, ≥99.5%). Curium additions were made using a 2.1×10^{-5} M stock (subsequently diluted four-fold) with an isotopic distribution of ^{248}Cm = 89.7% (remaining isotopes: ^{243}Cm = 0.4%, ^{244}Cm = 0.3%, ^{245}Cm = 0.1%, ^{246}Cm = 9.4%, ^{247}Cm = 0.1%).

2.2. pH measurements

A combination pH electrode (Orion Ross), freshly calibrated against standard pH buffers (pH = 4–12, Merck), was used for all pH measurements. Experimental pH (pH_{exp}) was corrected for proton activity (γ_{H+}) and electrolyte background (NaCl) effects on the electrode using the formula: $\log m_{H^+} = pH_{exp} + A$, where $-\log m_{H^+} = pH_m$ and A is an empirical correction factor entailing the activity coefficient of H^+ and the liquid junction potential of the electrode for a given background electrolyte concentration. A values previously reported in the literature for NaCl system were considered for the calculation of pH_m (Altmaier

et al., 2003).

2.3. Time-resolved laser fluorescence measurements and parallel factor analysis modelling

After preparation in an Ar-glove box using quartz cuvettes, samples were analyzed using TRLFS as a series of pH titrations (pH_m = 6–13) with $[cit]_T = 1$ mM and $[Cm]_T = 1.3 \times 10^{-7}$ M as initial concentrations. Solutions of NaCl–NaOH with I = 0.5 M were used to increase pH_m without altering the overall ionic strength of the sample. Citrate concentration (1 mM) was selected to ensure the predominance of the complex $Cm(cit)_2^{3-}$ at pH_m = 6, based on speciation calculations conducted with the thermodynamic selection in the NEA-TDB (Figure S1). This species is taken as an anchoring point in the development of a chemical model for the Cm(III)-cit system at higher pH_m values. Calcium titrations were performed on samples with fixed pH_m (5.0, 7.1, 8.9, 10.3, and 12.1), fixed cit (1 mM), and a starting Cm concentration of 1.6×10^{-7} M, with Ca = 0–50 mM. The upper limit of 50 mM was chosen based on the upper solubility limit defined by $Ca_3(cit)_2 \bullet 4H_2O(cr)$ under the conditions of this study. A minimum equilibration period of 4 h was allowed between sample preparation and measurement. Measurements of pH were made before and after each analysis.

TRLFS measurements were conducted with a pulsed Nd:YAG (Continuum Surelite II) pumped dye laser system using an excitation wavelength of λ = 396.6 nm, a spectral window of 580–620 nm, and an input side slit width of 2500 nm. Where appropriate, a duplicate spectrum was collected with the spectral window shifted to 590–630 nm to check for additional peaks. A gate delay of 20 ns and gate width of 1 ms were used. Gate delay steps varied from 15 to 50 μs for fluorescence lifetimes. The fluorescence emission lifetime, τ, of each sample was determined by fitting the area of the experimental integrated fluorescence intensity (I) at time, t, to the exponential decay equation $I(\lambda) = I_0(\lambda) \cdot e^{(-t/\tau)}$. The number of coordinated water molecules to curium in aqueous solution was calculated using its relationship to the fluorescence decay constant, k_{obs}, by $nH_2O = 0.65k_{obs} - 0.88$ (Kimura and Choppin, 1994). More details regarding the lifetime fitting procedure are described in Figure S2.

A series of TRLFS data were acquired over a pH range of 5.0–12.5 and preprocessed to correct for background noise through baseline subtraction, intensity-normalized using a min-max method from 0 to 1, and normalized to a laser power of 12 mW. Due to the low concentration of Cm, inner-filter effects were considered negligible. The preprocessed data formed a three-dimensional tensor ($13 \times 1024 \times 16$), denoted as $\underline{\mathbf{X}}$, representing pH, wavelength, and delay time dimensions, respectively. The PARAFAC algorithm, implemented through the N-way toolbox for MATLAB®,(Andersson and Bro, 2000) was employed to analyze the multidimensional tensor $\underline{\mathbf{X}}$. A comprehensive description of PARAFAC is not within the scope of this article; instead, readers are directed to the literature (Bro, 1997) and the associated references therein for a thorough exploration of the topic. A brief introduction of PARAFAC is provided in the Supporting Information.

2.4. Density functional theory calculations

Quantum chemical calculations on the complexes were conducted using DFT-BP86 with the def2-TZVP basis set and the COSMO solvation model. We optimized the structures of these complexes with DFT (Hohenberg and Kohn, 1964; Kohn and Sham, 1965). We determined the equilibrium structures of the proposed complexes and calculated the vibrational frequencies at the optimized structures to ensure that there are no imaginary vibrational frequencies and the structure is, indeed, an equilibrium structure and not a saddle-point. As we are only interested in the equilibrium structures of the ground states, we employed DFT. The application of time-dependent (TD)-DFT, which is suited for excited states, was not required. Calculations were performed using TURBOMOLE (version 7.0, 2015) (Ahlrichs et al., 2015; Deglmann et al., 2004; Eichkorn et al., 1995, 1997; Schäfer et al., 1992; Treutler and Ahlrichs, 1995; Von Arnim and Ahlrichs, 1999) with the same functional and basis set as in our previous studies (DFT-BP86 (Ahlrichs et al., 2000), def2-SVP (Schäfer et al., 1992)) (Tasi et al., 2018a, 2018b; Szabo et al., 2022). For Cm(III), we used pseudopotentials (PP) and the corresponding def-TZVP basis set, which considerably simplified the DFT calculations (Cao and Dolg, 2004).

As a simple minimal model for the proposed complexes, we included 15 water molecules and either 4 Na^+ or 2 Ca^{2+} counter ions in the first coordination sphere and optimized the structures of these systems with DFT calculations. Additional solvent effects beyond the first shell of solvent molecules were considered using the conductor-like screening model (COSMO) (Klamt and Schüürmann, 1993; Klamt, 1995; Baldridge and Klamt, 1997). Considering the first water/counter ions shell explicitly and dealing with additional solvation effects by means of COSMO provides a reasonable approach to investigate structures of species in solutions. These models should be considered as a rough approximation to study the possible existence of such complexes. A detailed study of these species in their chemical environment would require large scale and more sophisticated molecular dynamics (MD) calculations.

3. Results and discussion

3.1. TRLFS of aqueous curium(III)-citrate complexes

3.1.1. The binary Cm-cit system

Spectroscopic investigation of the Cm(III)-cit system was conducted as a function of pH to validate the current speciation regime and to determine the effect of Cm(III) hydrolysis on speciation under alkaline conditions. Fig. 1a shows Cm-cit emission spectra normalized to equal peak height, lifetime measurements, and, in Fig. 1b, water molecules in the Cm hydration sphere (calculated using the linear relationship to fluorescence decay from Kimura and Choppin (1994)) when pH_m = 5.0–12.5. Evidence of complexation was given by a bathochromic shift of the Cm aquo ion peak from 593.7 to 599.5 nm and a decrease in nH_2O from 8.6 to 4.5 in the presence of 1 mM cit at pH_m 5.0. The observed increase in luminescence lifetime of Cm-cit at higher pH_m values is attributed to the replacement of quenching water molecules by functional groups of citrate in the inner coordination sphere of curium. The extent of the lifetime increase depends on the degree of complexation and the coordination mode adopted by the citrate ligands, which can modulate the non-radiative deactivation pathways involving vibrational energy transfer to the water molecules and the luminescence efficiency of curium. Our spectra are in reasonable agreement with Heller et al. (2012), but the values for nH_2O at pH 12.5 are disparate, possibly due to precipitation or Cm sorption to the cuvette wall in the Heller et al. (2012) study, suggested by their low intensity and starting concentration of $[cit]_T$ = 0 M. Similar results are described for Cm-gluconate TRLFS at pH 12, where Rojo et al. (2021) propose Cm sorption or precipitation at lower gluconate concentrations. We likewise observed low Cm emission intensity in the present work when starting with 0 M cit, even after increasing the cit concentration to 5 mM. Sorption was, thus, less pronounced in the present work by starting with Cm-cit complexes at $[cit]_T$ = 1 mM and pH_m 5.7 and subsequently increasing pH.

A 3-nm bathochromic shift was observed between spectra at pH_m 5.0 and 7.0, where current speciation calculations using selected stability constants from Hummel et al. (2005) predict $Am(cit)_2^{3-}$ as the only predominant species in this pH range (Figure S1b). While it is known that the onset of the first Cm hydrolysis product begins around pH_m 6 and becomes predominant at pH_m 8 in the absence of citrate, (Guillaumont et al., 2003; Wimmer et al., 1992; Neck et al., 2009) it is unlikely that the observed bathochromic shift from 599.5 to 602.4 nm would represent a ternary Cm–OH–cit complex, as citrate is likely to decrease the Lewis acidity of Cm, thus delaying the onset of hydrolysis for the Cm-cit complex. Given that the second Cm hydrolysis product (λ

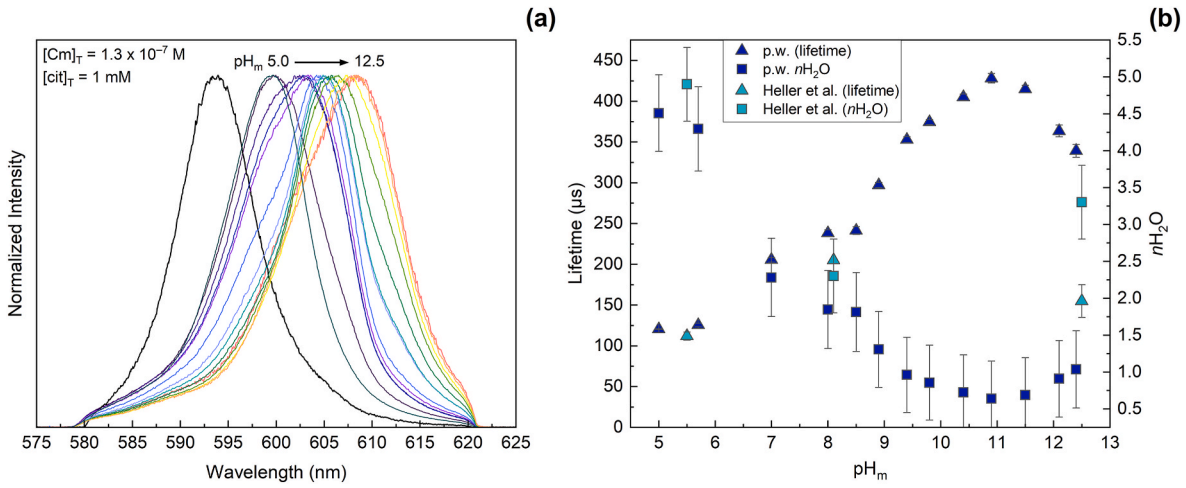


Fig. 1. Normalized Cm(III) fluorescence spectra (a) and lifetime measurements (left y-axis, triangles) and calculated number of coordinated water molecules (right y-axis, squares) (b) as a function of pH in the presence of $[cit]_T = 1$ mM, at approximately 0.5 pH unit intervals, from pH_m 5.0 to 12.5. The Cm(III) aquo ion in 0.5 M NaCl is given by the bold black line (pH_m 2.9). $I = 0.5$ M Na–Cl–OH-cit. Spectra were normalized using a min-max method from 0 to 1. Uncertainty was propagated using the uncertainty associated with the lifetime fit and the ±0.5 $n H_2O$, as determined by Kimura and Choppin (Kimura and Choppin, 1994).

= 603.5 nm)(Fanghänel et al., 1994) does not form until $pH_m > 7$ (and isn't predominant until pH_m 8), (Guillaumont et al., 2003; Fanghänel et al., 1994) it is likely that, especially if the stoichiometry of Cm-cit complexes remains the same between pH_m 5 and 7 (per the NEA-TDB), (Hummel et al., 2005) the manner of citrate coordination to Cm must change between pH_m 5 and 7. Furthermore, from pH_m 6, the normalized fluorescence spectra acquired at increasing delay times were characterized by an asymmetric narrowing of the emission bands and a slight red-shift. The left side of the peak gradually became narrower at longer delay times, while the right side remained relatively unchanged (Figure S3a). This asymmetric behavior suggests that (1) the overall luminescence decay is composed of contributions from multiple emitting species with distinct luminescence characteristics and lifetimes and (2) there is a subtle change in the ligand field environment experienced by Cm, which is attributed to the presence of slightly varied coordination geometries. Nonetheless, a mono-exponential fit was successfully applied to model the decay process (Table S2), which indicates a fast ligand exchange between the two excited species compared to the radiative decay rate of the excited states. This fast exchange can be attributed to the similar coordination environments and energetics involved.

We hypothesize, based on studies with di- and trivalent metals (Strouse, 1977; Hedwig et al., 1980; Baker et al., 1983; Öhman, 1988; Kieboom et al., 1977; Chunbo et al., 1995; Silva et al., 2009b; Motekaitis and Martell, 1984; Clausén et al., 2005; Jackson and du Toit, 1991), that citrate may convert from a bidentate to a tridentate coordination mode involving a terminal carboxylate and the central carboxylate and hydroxyl groups. Tridentate coordination of one or both citrate molecules to Cm is further supported by the value of 2.3 for $n H_2O$ at pH_m 7.0, a decrease of approximately $2 H_2O$ from pH_m 5.0.

Continued bathochromic shift and a decrease in $n H_2O$ was observed until pH_m 10.9, ultimately reaching the lowest observed value of $n H_2O = 0.6$, suggesting further involvement of the citrate hydroxyl in coordination to Cm. Heller and co-workers proposed the predominance of the complex $Cm(H_{-1}cit)_2^{5-}$ at pH 12.5,[49] but reported a lifetime of 155 ± 20 µs, corresponding to a difference of nearly 3 coordinated waters compared to the present study (see Fig. 2b). This discrepancy can be attributed to the presence of sorbed or precipitated species, as mentioned earlier. The low intensity of the pH 12.5 sample in the previous study may have further contributed to erroneous lifetime calculations for the $Cm(H_{-1}cit)_2^{5-}$ species. Note further that for this specific sample, the authors indicated that the lifetime and corresponding $n H_2O$ value were "reported with reservations since only two analyzable spectra were measured." Additionally, rather than mention of citrate alcohol involvement, chemically equivalent hydrolyzed Am or Cm-cit complexes have also been postulated, typically involving only one citrate moiety (Moutte and Guillaumont, 1969; Bouhlassa and Guillaumont, 1984; Eberle and Moattar, 1972; Hummel, 1993). Moutte and Guillaumont (1969) are the only previous authors to mention hydrolyzed complexes containing two citrate moieties, including $Cm(OH)(cit)_2^{4-}$ and $Cm(OH)_2(cit)_2^{5-}$, but they find no experimental evidence for the latter complex, presumably because of the limited pH range of their study (pH ≤ 8). We did not see evidence for the chemical equivalent species ($Cm(H_{-1}cit)_2^{5-}$) until pH > 9.

Though peak maxima exhibited continued bathochromic shift until pH_m 12.5, reaching a cumulative peak center at $\lambda = 608.5$ nm, a shoulder peak began growing in around $pH_m = 10.9$, likely attributable to hot bands (Lindqvist-Reis et al., 2005). The increase in $n H_2O$ for $pH_m > 11$ may indicate OH^- competition for the Cm metal center, eventually removing one citrate from the complex, as in $Cm(OH)_x(H_{-1}cit)^{-x}$ (Rabung et al., 2008). Additional work as a function of citrate concentration for $pH_m > 12$ may elucidate the nature of citrate and OH^- competition for Cm under hyperalkaline conditions.

3.1.2. *The ternary Ca-Cm-cit system*

Investigations of Cm-cit complexes were carried out at fixed pH_m as a function of calcium concentration to probe for potential ternary Ca-Cm-cit complexes. Fig. 2 shows emission spectra for samples with pH_m from 5.0 to 12.1 and $[Ca]_T = 0$–50 mM. A pronounced bathochromic shift was observed for samples with $pH_m = 5.0$ and 7.1, suggesting the presence of multiple distinct species with increasing calcium concentrations. The dominant peak at pH_m 7.1 and $[Ca]_T = 20$ mM, attributed to a ternary Ca-Cm-cit species, had a maximum at 605 nm—about a 5-nm red-shift from the Ca-free sample. Regardless of hydroxyl coordination, each citrate moiety in a 1:2 Cm-cit complex would have at least one uncoordinated carboxylate group, which is thus available for complexation with Ca.

Some estimates can be made regarding the coordination of the Ca-Cm-cit complexes based on the TRLFS spectra. In addition to a bathochromic shift, the calculated number of coordinated waters decreased from 4.5 to 3.1 and 3.1 to 2.3 for samples with $pH_m = 5.0$ and 7.1, respectively, from $[Ca]_T = 0$–50 mM (Fig. 2f–Table S3). One possible explanation for this phenomenon could be the coordination of the Cm ion with a deprotonated alcohol group of citrate. Hence, the coordination with Ca is expected to enhance the acidity of the alcohol group, resulting in deprotonation at a lower pH compared to Ca-free systems.

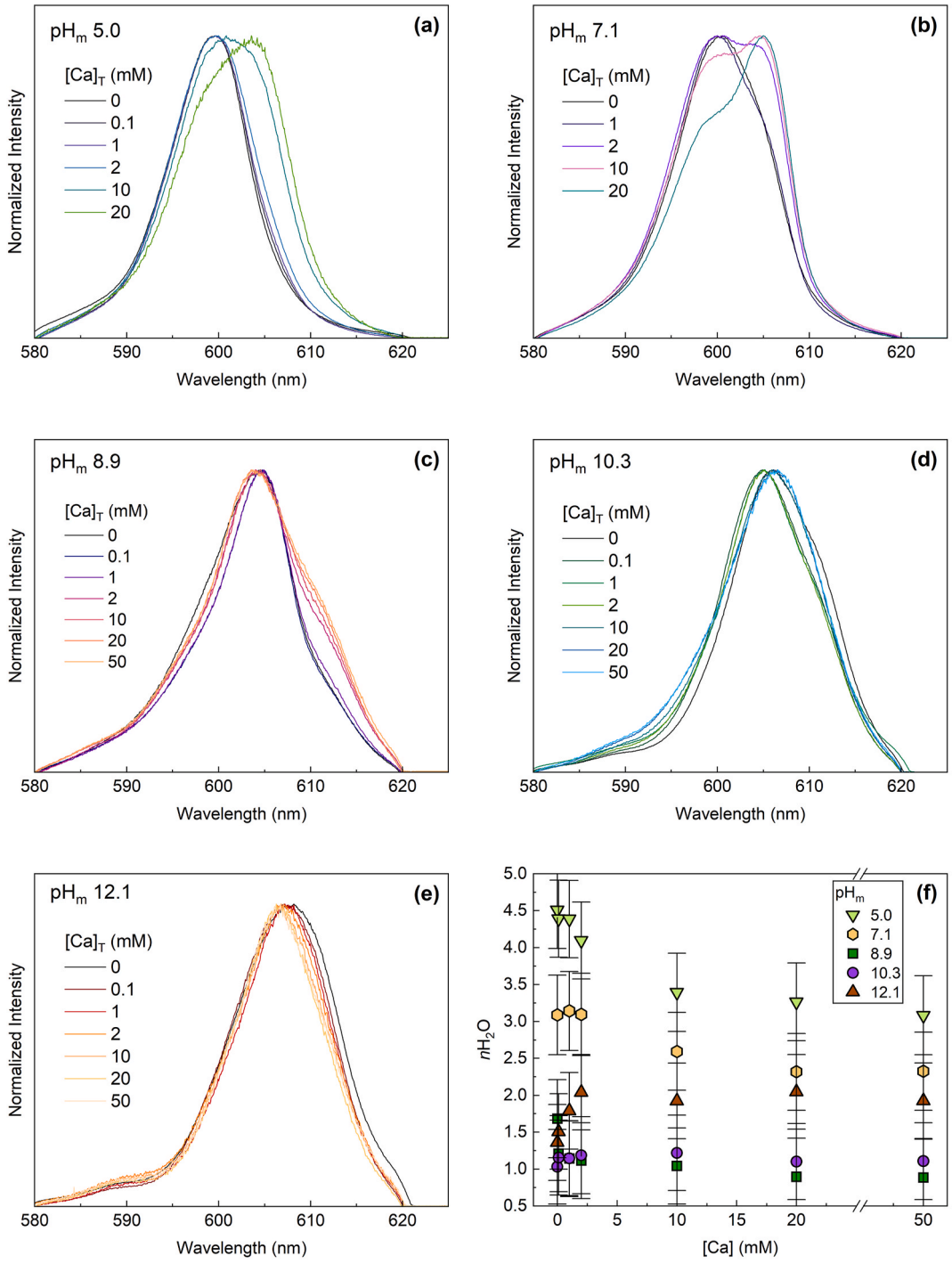


Fig. 2. Normalized Cm(III) fluorescence spectra as a function of calcium concentration (0–20 or 0–50 mM) at fixed pH_m values (a–e) and their associated emission lifetime measurements (f), all in the presence of $[cit]_T = 1$ mM and $I = 0.5$ M Ca–Na–Cl–OH-cit. Initial $[Cm]_T = 1.6 \times 10^{-7}$ M. Spectra were normalized using a min-max method from 0 to 1. Uncertainty was propagated using the uncertainty associated with the lifetime fit and the ± 0.5 nH$_2$O, as determined by Kimura and Choppin (Kimura and Choppin, 1994).

Samples with $pH_m \geq 8.9$ had peak centers that would overlap the 605 nm peak associated with a ternary Ca-Cm-cit complex, but some preliminary assessments can still be made about these higher-pH Ca-bearing samples. Notably, a shoulder at ~612 nm appears in the pH_m 8.9 sample with increasing Ca, suggesting a new ternary Ca-Cm-cit or quaternary Ca-Cm–OH–cit species. In the absence of calcium, we do not see evidence for $Cm(cit)(H_{-1}cit)^{4-}$ and $Cm(H_{-1}cit)_2^{5-}$ until pH_m 7.0 and 9.4, respectively. However, if incorporation of calcium into these complexes lowers the Lewis basicity of citrate, thus advancing the pH at which citrate alcohol coordination to Cm occurs, it is possible that the shoulder at ~612 nm can be attributed to either deprotonation of the second citrate alcohol group (e.g., $Ca_2Cm(H_{-1}cit)_2^-$) or hydrolysis of a Ca-Cm-cit species (e.g., $Ca_2Cm(OH)(cit)(H_{-1}cit)^-$). Either scenario is supported by lifetime measurements of this sample, where a loss of 0.8 water molecules was observed between $[Ca]_T = 0$–50 mM.

Changes in spectra at pH_m 10.3 with increasing calcium were more subtle (due to overlapping peaks), but at higher calcium concentrations, equilibrium between binary Cm-cit and ternary Ca-Cm-cit complexes is

speculated. A gradual hypsochromic shift was observed for pH_m 12.1 spectra with increasing Ca, likely signaling a shift in predominance of $Cm(H_{-1}cit)_2^{5-}$ to a mixture also containing ternary Ca-Cm-cit complex (es). As was seen in the binary Cm-cit system, lifetimes in the presence of Ca increased by almost 1.0 nH_2O as the pH_m increased from 8.9 to 12.1, which may indicate concurrence of Cm hydrolysis species and minor contributions from ternary Ca-Cm-OH species (Rabung et al., 2008).

3.2. PARAFAC decomposition of the binary Cm-cit system

Parallel factor analysis (PARAFAC)(Andersson and Bro, 2000) was used to deconvolute pure components of the Cm-cit system. The core consistency (CC) diagnostic and the sum of squared residuals (SSR) were calculated as a function of the number of factors, as shown in Table S4. A three-component system was determined to be the most reliable, to which we assigned the generic naming scheme "Species 1," "Species 2," and "Species 3". The pure spectral components derived from PARAFAC can be found in Fig. 3, along with an example fit using these components. Successive fitting iterations were conducted with the percent components suggested by PARAFAC until a reduction in chi-squared values was observed.

The lifetimes determined with PARAFAC were 125.8 ± 0.4, 356 ± 4.5, and 405 ± 0.5 μs for Species 1, Species 2, and Species 3, respectively, which correspond to 4.3, 0.9, and 0.7 coordinated water molecules. We note that Species 2 and 3 have similar lifetimes, which may correspond to similar chemical environments of the Cm ion, as suggested by DFT calculations. Still, the structures of the two complexes are different enough to produce the observed bathochromic shift with increasing pH, and suggest a possible limitation of the linear relationship determined by Kimura and Choppin (1994). Another example of distinct bathochromic shift with little influence on lifetime measurements is found in the Cm–F TRLFS study by Skerencak et al. (2010) where the authors used DFT to demonstrate that fluoride pulls waters from the second coordination sphere closer to Cm, resulting in increased fluorescence quenching. The lifetime remained at 65 μs, despite clear evidence for additional Cm–F species.

Fraction species calculations (Fig. 4a) using PARAFAC-derived component analysis demonstrated the predominance of Species 2 from pH_m 8–10, a 50-50 mixture of Species 2 and Species 3 at pH_m 10.4, and the subsequent predominance of Species 3 at $pH_m > 10.4$. Pure component spectra were fit to experimental spectra according to the fraction species shown in Fig. 4a, assuming the coordination and deprotonation of one citrate alcohol group occurred with each successive species. Multiple iterations of the spectral fits were then performed to improve the fit and subsequent chi-squared values. Calculated fluorescence intensity factors did not result in improved spectral fits and were, thus, considered unity in the present study. Slope analysis as a function of pH_m (Fig. 4b) revealed a reasonable agreement to a slope = 1 for the formation of each species pair with increasing pH, supporting the loss of one proton in the stepwise complexation reactions. Considering the predominance of $Cm(cit)_2^{3-}$ at $pH_m = 5$ and $[cit]_T = 1$ mM as an anchoring point (as calculated using the NEA-TDB selection), we conclude that the subsequent species dominating the aqueous speciation of Cm(III) are $Cm(cit)(H_{-1}cit)^{4-}$ and $Cm(H_{-1}cit)_2^{5-}$. Note that the predominance of these species is only claimed at $[cit]_T = 1$ mM (i.e., large excess of citrate). Other species with a Cm:cit ratio of 1:1, as well as possible hydrolysis of 1:1 species, are likely to form at lower ligand concentration regimes instead of the proposed 1:2 complexes.

3.3. Theoretical molecular modeling using DFT

Quantum chemical calculations were conducted using DFT(BP86)/def2-TZVP and optionally with the COSMO solvation model. Both theoretical facets support the predicted $Cm(cit)_2^{3-}$, $Cm(cit)(H_{-1}cit)^{4-}$, and $Cm(cit)_2^{5-}$ complexes as having the lowest energy minima and provide bond distances in close agreement with one another (with deviations ≤ 4 pm). Each complex possessed a coordination number of 8 and was embedded in four $[Na(H_2O)_4]^+$ groups, resulting in net charges of +1, 0, and −1 for $Cm(cit)_2^{3-}$, $Cm(cit)(H_{-1}cit)^{4-}$, and $Cm(H_{-1}cit)_2^{5-}$, respectively. The structure of the $Cm(cit)(H_{-1}cit)^{4-}$ complex, as calculated with DFT, is illustrated in Fig. 5a. Hydrolysis of water, in lieu of deprotonation of one citrate hydroxyl group, becomes more feasible for the curium ion in the case of $Cm(cit)_2^{5-}$, but this complex was still found to have a slightly lower energy than $Cm(OH)(cit)(H_{-1}cit)^{5-}$, suggesting that the predominance of hydrolyzed Cm-cit species under alkaline conditions is less likely. We speculate that such hydrolyzed species form at higher pH values than those investigated in this work, or otherwise at lower ligand concentrations, where 1:1 complexes form and, thus, a greater number of water molecules are directly coordinated to the Cm^{3+} ion.

Deprotonated alcohol groups exhibited the strongest Cm-cit interaction, evidenced by the shortest bond distances (see Table 1). Participation of protonated citrate alcohol groups in the inner Cm coordination sphere is still predicted for $Cm(cit)_2^{3-}$, given their calculated Cm–O bond distances of 246.2 and 250.4 p.m., which are slightly longer than the Cm–O distances to the carboxylate groups (234.7–250.9 pm). The carboxylate bond distances increased with each complex as the alcohols became deprotonated, further highlighting the favorability of alcohol coordination, with the closest Cm–COO^- distance being 234.7 and 239.7 pm for $Cm(cit)_2^{3-}$ and $Cm(H_{-1}cit)_2^{5-}$, respectively. It was also found that

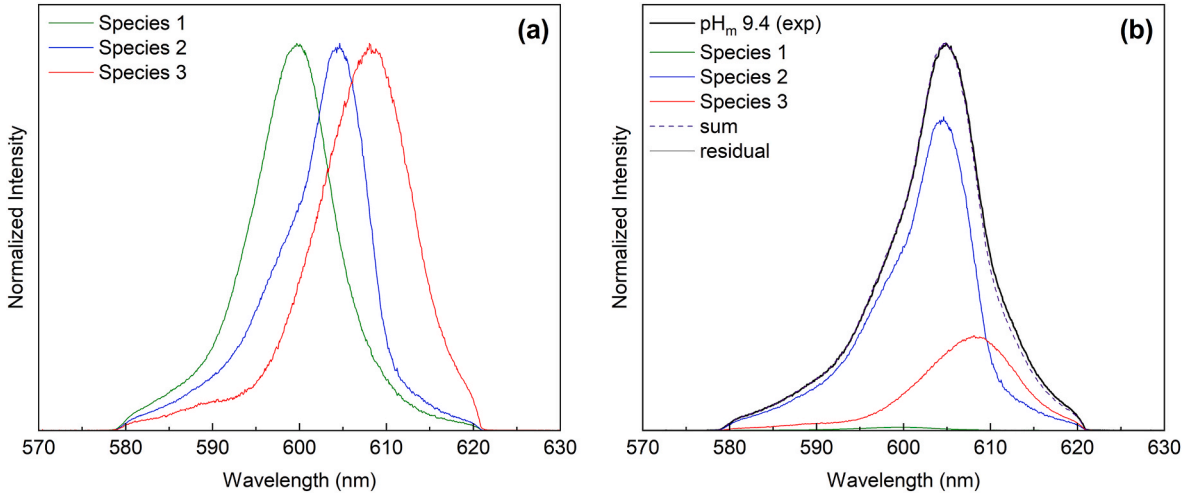


Fig. 3. Pure spectral components derived from PARAFAC (a) and example fit of experimental pH_m 9.4 spectrum using the PARAFAC-derived components (b).

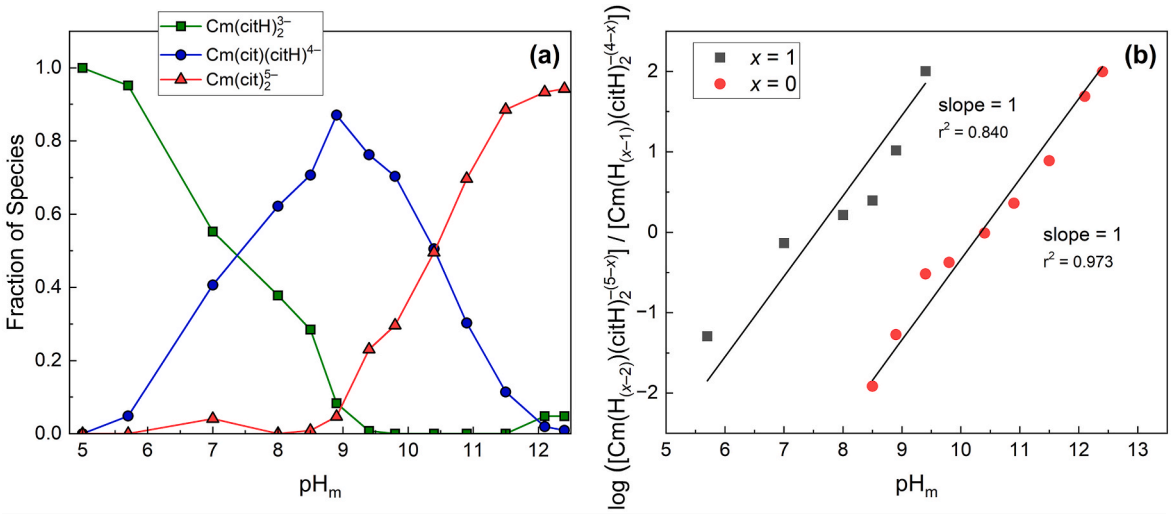


Fig. 4. Fraction species derived from PARAFAC, assuming deprotonation of 1 and 2 citrate alcohol groups for Species 2 and 3, respectively (a) and slope analysis of the three components as a function of pH_m, corresponding to log molarity of ($[Cm(H_{(x-2)})(cit)_2^{-(5-x)}]/[Cm(H_{(x-1)})(cit)_2^{-(4-x)}]$), where $x = 1, 0$ (b). Lines in (a) are meant to guide the eye.

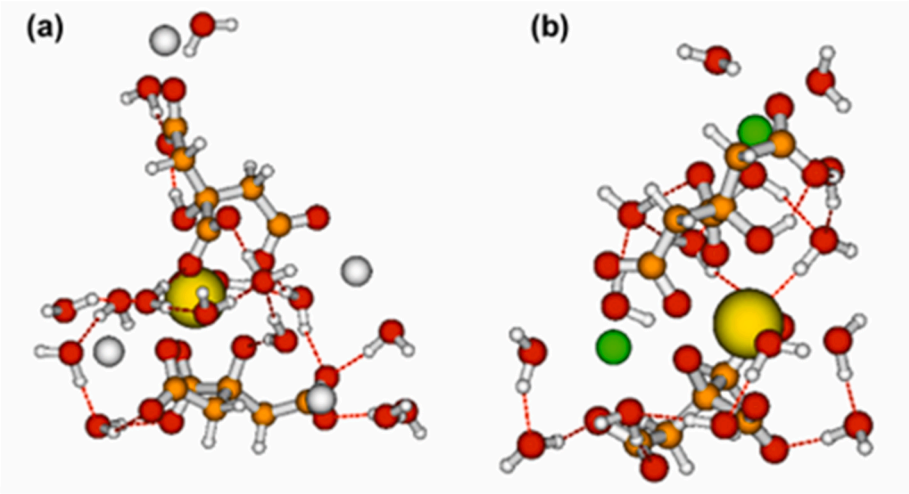


Fig. 5. DFT-calculated structures of $Na_4[Cm(cit)(H_{-1}cit)](aq)$ (a) and $Ca_2[Cm(cit)(H_{-1}cit)](aq)$ (b). Legend: curium: yellow, sodium: grey, calcium: green, carbon: orange, oxygen: red, hydrogen: white. Red dashed lines indicate hydrogen bonding. (For interpretation of the references to colour in this figure legend, the reader is referred to the Web version of this article.)

Table 1
Calculated Cm–O bond distances for binary Cm-cit complexes using DFT (def2-TZVP/BP86). COO^- = carboxylate, CO^- = alcohol. Distances are given in pm.

Species	COO^-	COO^-	COO^-	COO^-	CO^-	CO^-	H_2O	H_2O
$Cm(cit)_2^{3-}$	234.7	235.7	243.5	251.0	246.2	250.4	250.5	257.2
$Cm(cit)(H_{-1}cit)^{4-}$	239.9	245.5	246.7	247.0	225.1	255.1	257.7	260.1
$Cm(H_{-1}cit)_2^{5-}$	239.7	244.1	244.9	255.6	225.9	234.9	269.4	277.5

the Cm–H_2O distances increased with each alcohol deprotonation, ranging from 250.5 to 257.2 pm for $Cm(cit)_2^{3-}$ to 269.4 and 277.5 pm for $Cm(H_{-1}cit)_2^{5-}$. These longer Cm–H_2O distances support our observations of increasing fluorescence lifetimes with increasing pH, as $Cm(cit)(H_{-1}cit)^{4-}$ and $Cm(H_{-1}cit)_2^{5-}$ become more predominant: We would already expect displacement of water molecules in the Cm hydration sphere upon coordination of the citrate alcohol group, but an increased Cm–H_2O distance may further inhibit quenching by OH oscillations from nearby waters, which may explain the $nH_2O < 1$ seen for samples with $10 \leq pH \leq 12$ and the increased lifetimes determined by PARAFAC for $Cm(cit)(H_{-1}cit)^{4-}$ and $Cm(H_{-1}cit)_2^{5-}$. This highlights a limitation of the linear equation used to derive the number of inner sphere waters for Cm determined by Kimura and Choppin (1994) as it does not factor in Cm–H_2O distances. In this case, we observed structural changes in the Cm coordination environment between $Cm(cit)(H_{-1}cit)^{4-}$ and $Cm(H_{-1}cit)_2^{5-}$, evidenced by bathochromic shift and DFT calculations, but the lifetimes, including those determined by PARAFAC, were less telling of the nature of each complex.

DFT calculations also support the formation of ternary Ca-Cm-cit complexes (Fig. 5b), where two Ca^{2+} serve to charge-stabilize instead of four Na^+. Like the binary complexes, a CN = 8 was assigned to each ternary complex. Regardless of alcohol coordination, two calcium ions

were found to be stable within each complex. For all three species, $Ca_2[Cm(cit)_2]^+$, $Ca_2[Cm(cit)(H_{-1}cit)](aq)$, and $Ca_2[Cm(H_{-1}cit)_2]^-$, there are shared carboxylate groups between calcium and curium with Ca–O bond distances ranging from 243.0 to 249.3 pm (Table 2). The $Ca_2[Cm(H_{-1}cit)_2]^-$ complex was found to have two shared alcohol groups, in addition to two shared carboxylate groups, between Ca and Cm. A greater number of shared functional groups likely enhances the overall stability of these complexes. Note that although the number of coordinated Ca atoms has been fixed to 2 in this exercise, the formation of complexes involving 1 or 3 Ca atoms can be also envisaged, depending also on the overall Ca concentration and ionic strength. Future work is warranted to better constrain the stoichiometry of these complexes, and to determine their stability constants and ionic strength dependence for use in thermodynamic and geochemical model calculations.

3.4. Proposed chemical model for the binary Cm-cit system

The evidence obtained in the present work, which includes a correlated slope = 1 for our 3-component Cm-cit system, suggests the predominance of $Cm(cit)_2^{3-}$ from pH_m 5.0–7.0, $Cm(cit)(H_{-1}cit)^{4-}$ from 7.0 < pH_m < 10.5, and $Cm(H_{-1}cit)_2^{5-}$ for pH_m > 10.5 in the presence of excess citrate. Similar findings were highlighted in Moutte and Guillaumont (1969) who propose a $Cm(OH)(cit)_2^{4-}$ complex that becomes predominant with $[cit]_T$ > 0.5 mM at pH 8. We have demonstrated, however, that deprotonation of the citrate hydroxyl group is more favorable, and, therefore, the complex that the authors are referring to is $Cm(cit)(H_{-1}cit)^{4-}$. Eberle and Moattar (1972) proposed the formation of $Am(H_{-1}cit)^-$ or $Am(OH)(cit)^-$ for pH > 6 based on spectrophotometric measurements. However, given the >50-fold excess of citrate used in their study, it is more probable for their proposed complex to possess two citrate moieties. The authors provide an absorption spectrum of $[Am]_T$ = 1.8 mM and $[cit]_T$ = 100 mM at pH 9.28. The > 3-nm red-shift exhibited between pH 6.12 and 9.28 agrees with similar spectroscopic observations for Cm-cit in the present study. The pH 9.28 spectrum from Eberle and Moattar also exhibits a shoulder of approximately similar predominance as the proposed fraction species of $Cm(cit)(H_{-1}cit)^{4-}$ and $Cm(H_{-1}cit)_2^{5-}$ in the present work (Fig. 3b).

Further evidence is given for citrate hydroxyl coordination and deprotonation in Jackson and du Toit, 1991, where the authors used approximately equimolar concentrations (4–8 mM) of Gd and cit in combination with potentiometry and ^{13}C NMR to investigate the formation of $Gd(H_{-1}cit)^-$ above pH 5, establishing a tridentate configuration for citrate involving the hydroxyl group. In this study, the authors also indicate the formation of $Gd(OH)(H_{-1}cit)^{2-}$, which becomes predominant above pH 8.

Tamain et al. (2020) used a suite of analytical techniques, including ultraviolet–visible (UV–Vis) and nuclear magnetic resonance (NMR) spectroscopies, TRLFS, DFT, capillary electrophoresis, and extended X-ray absorption fine structure (EXAFS) to investigate Am-cit complexation at pH 1 and 3. The authors suggest that alcohol coordination/deprotonation occurs at pH 1 for 1:1 and 1:2 Am-cit complexes, but no alcohol involvement was inferred for pH 3 complexes. As mentioned by Tamain et al. (2020), a pH of 1 may be too low to allow for the deprotonation of additional carboxylate groups, and, instead, the hydroxyl group enters the Am coordination sphere. The observations described in Tamain et al. (2020) for pH 3 are in agreement with those described in the present work, where we have no evidence of citrate hydroxyl involvement at pH 5.

Finally, Heller et al. (2012) report the only other previously known Cm-cit TRLFS study (combined with DFT and FT-IR), where the authors used variable $[cit]_T$ up to 1 mM at multiple fixed pH values, from 2.4 to 12.5. Based on their combined DFT and FT-IR results, the authors correctly assume that the citrate hydroxyl group becomes coordinated to Cm and deprotonates with increasing pH. Up to pH 8.1, the spectra and calculated lifetimes agree with those observed in the present work. However, due to their method of starting with no ligand at pH 12.5, their results at such high alkalinity are likely overcome by irreversible sorption to the cuvette and/or precipitation, which was observed and subsequently avoided in the present work by increasing the pH of a solution already containing Cm and excess citrate. (In fact, this method was applied to a sample in the work of Heller et al. (2012) shown in their supplementary information, where a sample containing 1 mM cit was titrated up to pH 12.3 and can be seen to match our observed TRLFS spectra more closely, with $\lambda_{max} \approx 608$ nm) The authors nevertheless propose a model where $Cm(cit)_2^{3-}$ is predominant from 6 < pH < 9 and $Cm(H_{-1}cit)_2^{5-}$ becomes predominant above pH 9. The deviation between this speciation scheme and the one proposed in the present study may stem from the absence of $Cm(cit)(H_{-1}cit)^{4-}$ in Heller et al. (2012). The deprotonation of both alcohol groups in one step, as proposed by Heller et al. (2012) is unlikely and contradicts our own observations. Such a reaction would likely manifest as a distinct isosbestic point in the TRLFS spectra, which was not observed here. Thus, we propose the stepwise coordination and deprotonation of the citrate alcohol groups as the most plausible fit for our combined emission spectra, lifetimes, multi-way decomposition and slope analysis, and quantum chemical investigation. Note, however, that behavior in a lower ligand concentration regime (i.e., roughly equimolar Cm:cit concentrations) may differ, in that the formation of ternary complexes $Cm(OH)_x(H_{-1}cit)^{-x-1}$ is expected under hyperalkaline pH conditions, as demonstrated in Jackson and du Toit, 1991 for Gd.

4. Conclusions

We provided an updated speciation regime for the binary Cm-cit system under neutral to hyperalkaline conditions that defines the stoichiometry and demonstrates successive coordination and deprotonation of the citrate alcohol groups with increasing pH. This, along with knowledge of newly described ternary Ca-Cm-cit species, sets the basis for new thermodynamic studies to come and future applications modeling the chemical behavior of An(III) under geochemical conditions of relevance for environmental applications and in the context of repositories for nuclear waste disposal.

CRediT authorship contribution statement

Matthew B. Comins: Writing – review & editing, Writing – original draft, Visualization, Investigation, Formal analysis. **Chengming Shang:** Writing – review & editing, Supervision, Formal analysis, Conceptualization. **Robert Polly:** Writing – review & editing, Formal analysis. **Andrej Skerencak-Frech:** Writing – review & editing, Supervision. **Marcus Altmaier:** Writing – review & editing, Supervision. **Amy E. Hixon:** Writing – review & editing, Supervision. **Xavier Gaona:** Writing

Table 2
Calculated Cm–O and Ca–O bond distances for shared functional groups within ternary Ca-Cm-cit complexes using DFT (def2-TZVP/BP86). COO^- = carboxylate, CO^- = alcohol. Distances are given in pm.

Species	COO^-	COO^-	COO^-	COO^-	CO^-	CO^-	CO^-	CO^-
	Cm–O	Ca–O	Cm–O	Ca–O	Cm–O	Ca–O	Cm–O	Ca–O
$Ca_2Cm(cit)_2^+$	240.5	246.3						
$Ca_2Cm(cit)(H_{-1}cit)(aq)$	239.0	244.8						
$Ca_2Cm(H_{-1}cit)_2^-$	238.8	249.3	240.2	243.0	229.4	233.0	242.4	239.6

– review & editing, Supervision, Project administration, Conceptualization.

Declaration of competing interest

There is nothing to declare.

Data availability

A link to data can be found at the attached file step.
Curium citrate TRLFS, PARAFAC, DFT (Original data) (Mendeley Data)

Acknowledgements

This research was supported, in part, by an appointment to the DOE Scholars Program, administered by the Oak Ridge Institute for Science and Education and funded by the WIPP Project (DOE-CBFO). We are grateful to Tobias Hippel for help with TRLFS measurements and to technical staff that support and maintain the safe operation of the controlled area within KIT-INE. The authors acknowledge support by the state of Baden-Württemberg through bwHPC and the German Research Foundation (DFG) through grant no. INST 40/575-1 FUGG (JUSTUS 2 cluster).

Appendix A. Supplementary data

Supplementary data to this article can be found online at https://doi.org/10.1016/j.chemosphere.2024.143233.

References

Ahlrichs, R., Furche, F., Grimme, S., Comment on "'Assessment of Exchange Correlation Functionals, 2000. [A.J. Cohen, N.C. Handy, Chem. Phys. Lett 316, 160–166. Chem. Phys. Lett. 2000, 325, 317–321.

Ahlrichs, R., Furche, F., Hättig, C., Klopper, W.M., Sierka, M., Weigend, F., 2015. TURBOMOLE v7.0.

Altmaier, M., Metz, V., Neck, V., Müller, R., Fanghänel, Th, 2003. Solid-liquid equilibria of Mg(OH)2(Cr) and $Mg_2(OH)_3Cl{\cdot}4H2O$(Cr) in the system Mg-Na-H-OH-Cl-H_2O at 25°C. Geochem. Cosmochim. Acta 67 (19), 3595–3601. https://doi.org/10.1016/S0016-7037(03)00165-0.

Altmaier, M., Gaona, X., Fellhauer, D., Clark, D.L., Runde, W.H., Hobart, D.E., 2019. Aqueous solution and coordination chemistry of plutonium. In: Clark, D.L., Geeson, D.A., Hanrahan, R.J. (Eds.), Plutonium Handbook, vol. 3, pp. 1543–1726.

Andersson, C.A., Bro, R., 2000. The N-way toolbox for MATLAB. Chemometr. Intell. Lab. Syst. 52 (1), 1–4. https://doi.org/10.1016/S0169-7439(00)00071-X.

Aoyagi, N., Palladino, G., Nagasaki, S., Kimura, T., 2018. Optical properties of trinuclear citrate complexes containing 4f and 5f block metals. Bull. Chem. Soc. Jpn. 91 (6), 882–890. https://doi.org/10.1246/bcsj.20170419.

Baker, E.N., Baker, H.M., Anderson, B.F., Reeves, R.D., 1983. Chelation of nickel(II) by citrate. The crystal structure of a nickel-citrate complex, $K_2[Ni(C_6H_5O_7)(H_2O)_2]_2{\cdot}4H_2O$. Inorg. Chim. Acta. 78, 281–285.

Baldridge, K., Klamt, A., 1997. First principles implementation of solvent effects without outlying charge error. J. Chem. Phys. 106 (16), 6622–6633. https://doi.org/10.1063/1.473662.

Bouhlassa, S., Guillaumont, R., 1984. Complexes citriques et citrates D'AMERICIUM. J. Less Common. Met. 99, 157–171.

Bro, R., 1997. PARAFAC. Tutorial and applications. Chemometr. Intell. Lab. Syst. 38, 149–171.

Bube, C., Metz, V., Bohnert, E., Garbev, K., Schild, D., Kienzler, B., 2013. Long-term cement corrosion in chloride-rich solutions relevant to radioactive waste disposal in rock salt – leaching experiments and thermodynamic simulations. Phys. Chem. Earth 64, 87–94. https://doi.org/10.1016/j.pce.2012.11.001.

Cao, X., Dolg, M., 2004. Segmented contraction scheme for small-core actinide pseudopotential basis sets. J. Mol. Struct.: THEOCHEM 673 (1–3), 203–209. https://doi.org/10.1016/j.theochem.2003.12.015.

Chunbo, Y., Juzheng, L., Daqing, Z., Yijie, W., Jiazuan, N., 1995. Lanthanide-induced shift and relaxation rate studies of the aqueous complexation of citrate. Polyhedron 14 (23–24), 3579–3583. https://doi.org/10.1016/0277-5387(95)00172-O.

Clausén, M., Öhman, L.-O., Persson, P., 2005. Spectroscopic studies of aqueous gallium (III) and aluminum(III) citrate complexes. J. Inorg. Biochem. 99 (3), 716–726. https://doi.org/10.1016/j.jinorgbio.2004.12.007.

Deglmann, P., May, K., Furche, F., Ahlrichs, R., 2004. Nuclear second analytical derivative calculations using auxiliary basis set expansions. Chem. Phys. Lett. 384 (1–3), 103–107. https://doi.org/10.1016/j.cplett.2003.11.080.

Eberle, S.H., Moattar, F., 1972. Die komplexe Des Am(III) mit zitronensäure. Inorg. Nucl. Chem. Lett. 8 (3), 265–272. https://doi.org/10.1016/0020-1650(72)80067-9.

Eichkorn, K., Treutler, O., Öhm, H., Häser, M., Ahlrichs, R., 1995. Auxiliary basis sets to approximate coulomb potentials. Chem. Phys. Lett. 240 (4), 283–290. https://doi.org/10.1016/0009-2614(95)00621-A.

Eichkorn, K., Weigend, F., Treutler, O., Ahlrichs, R., 1997. Auxiliary basis sets for main row atoms and transition metals and their use to approximate coulomb potentials. Theor. Chim. Acta 97 (1–4), 119–124. https://doi.org/10.1007/s002140050244.

Fanghänel, Th, Kim, J.I., Paviet, P., Klenze, R., Hauser, W., 1994. Thermodynamics of radioactive trace elements in concentrated electrolyte solutions: hydrolysis of Cm^{3+} in NaCl-solutions. Radiochim. Acta 66–67 (s1), 81–87.

Grenthe, I., Gaona, X., Plyasunov, A.V., Rao, L., Runde, W.H., Grambow, B., Konings, R.J. M., Smith, A.L., Moore, E.E., 2020. Second update on the chemical thermodynamics of uranium. NEPTUNIUM, PLUTONIUM, AMERICIUM AND TECHNETIUM 14.

Guidone, R.E., Gaona, X., Winnefeld, F., Altmaier, M., Geckeis, H., Lothenbach, B., 2024. Citrate sorption on cement hydrates. Cement Concr. Res. 178, 107404 https://doi.org/10.1016/j.cemconres.2023.107404.

Guillaumont, R., Fanghänel, T., Neck, V., Fuger, J., Palmer, D.A., Grenthe, I., Rand, M.H., 2003. Update on the chemical thermodynamics of uranium. NEPTUNIUM, PLUTONIUM, AMERICIUM AND TECHNETIUM 5, 959.

Hedwig, G.R., Liddle, J.R., Reeves, R.D., 1980. Complex Formation of nickel(II) ions with citric acid in aqueous solution: a potentiometric and spectroscopic study. Aust. J. Chem. 33, 1685–1693.

Heller, A., Barkleit, A., Foerstendorf, H., Tsushima, S., Heim, K., Bernhard III, G. Curium, 2012. Citrate speciation in biological systems: a europium(III) assisted spectroscopic and quantum chemical study. Dalton Trans. 41 (45), 13969 https://doi.org/10.1039/c2dt31480k.

Hicks, T.W., Baldwin, T.D., Hooker, P.J., Richardson, P.J., Chapman, N.A., McKinley, I. G., Neall, F.B., 2008. *Concepts for the geological Disposal of intermediate-level radioactive waste*; 0736–1; galson sciences limited. Nuclear Decommissioning Authority.

Hohenberg, P., Kohn, W., 1964. Inhomogeneous electron gas. Phys. Rev. 136 (3B), B864–B871. https://doi.org/10.1103/PhysRev.136.B864.

Hummel, W., 1993. ORGANIC COMPLEXATION of RADIONUCLIDES IN CEMENT PORE WATER: A CASE STUDY; INIS-MF-13636; Paul Scherrer Institute. Villigen, Switzerland, pp. 65–74.

Hummel, W., Anderegg, G., Rao, L., Puigdomènech, I., Tochiyama, O., 2005. Chemical Thermodynamics of compounds and complexes Of U, Np, Pu, Am, Tc, Se. Ni and Zr With Selected Organic Ligands 9, 1130.

Jackson, G.E., du Toit, J., 1991. Gadolinium(III) in vivo speciation. Part 1. A potentiometric and spectroscopic study of gadolinium(III) citrate complexes. J. Chem. Soc. Dalton Trans. 1463–1466.

Kieboom, A.P.G., Vijverberg, C.A.M., Peters, J.A., Van Bekkum, H., 1977. Complexation of acetate, glycolate, lactate, malate and citrate anions with lanthanide(III) cations in aqueous solution as studied by NMR spectroscopy. Recl. Trav. Chim. Pays-Bas 96 (12), 315–316. https://doi.org/10.1002/recl.19770961208.

Kimura, T., Choppin, G.R., 1994. Luminescence study on determination of the hydration number of Cm(III). J. Alloys Compd. 213–214, 313–317. https://doi.org/10.1016/0925-8388(94)90921-0.

Klamt, A., 1995. Conductor-like screening model for real solvents: a new approach to the quantitative calculation of solvation phenomena. J. Phys. Chem. 99 (7), 2224–2235. https://doi.org/10.1021/j100007a062.

Klamt, A., Schüürmann, G., 1993. COSMO: a new approach to dielectric screening in solvents with explicit expressions for the screening energy and its gradient. J. Chem. Soc., Perkin Trans. 2 (5), 799–805. https://doi.org/10.1039/P29930000799.

Kohn, W., Sham, L.J., 1965. Self-consistent equations including exchange and correlation effects. Phys. Rev. 140 (4A), A1133–A1138. https://doi.org/10.1103/PhysRev.140.A1133.

Kusbiantoro, A., Ibrahim, M.S., Muthusamy, K., Alias, A., 2013. Development of sucrose and citric acid as the natural based admixture for fly ash based geopolymer. Procedia Environ. Sci. 17, 596–602. https://doi.org/10.1016/j.proenv.2013.02.075.

Lindqvist-Reis, P., Klenze, R., Schubert, G., Fanghänel, T., 2005. Hydration of Cm^{3+} in aqueous solution from 20 to 200 °C. A time-resolved laser fluorescence spectroscopy study. J. Phys. Chem. B 109 (7), 3077–3083. https://doi.org/10.1021/jp045516+.

Möschner, G., Lothenbach, B., Figi, R., Kretzschmar, R., 2009. Influence of citric acid on the hydration of portland cement. Cement Concr. Res. 39 (4), 275–282. https://doi.org/10.1016/j.cemconres.2009.01.005.

Motekaitis, R.J., Martell, A.E., 1984. Complexes of aluminum(III) with hydroxy carboxylic acids. Inorg. Chem. 23 (1), 18–23. https://doi.org/10.1021/ic00169a006.

Moutte, A., Guillaumont, R., 1969. Complexes Citriques d'actinium et de Curium. Rev. Chim. Miner. 6 (3), 603–610.

Neck, V., Altmaier, M., Rabung, T., Lützenkirchen, J., Fanghänel, T., 2009. Thermodynamics of trivalent actinides and neodymium in NaCl, $MgCl_2$, and $CaCl_2$ solutions: solubility, hydrolysis, and ternary Ca-M(III)-OH complexes. Pure Appl. Chem. 81 (9), 1555–1568. https://doi.org/10.1351/PAC-CON-08-09-05.

Öhman, L.-O., 1988. Equilibrium and structural studies of silicon(IV) and aluminum(III) in aqueous solution. 17. Stable and metastable complexes in the system H^+–Al^{3+}–citric acid. Inorg. Chem. 27 (15), 2565–2570.

Rabung, T., Altmaier, M., Neck, V., Fanghänel, T., 2008. A TRLFS study of Cm(III) hydroxide complexes in alkaline $CaCl_2$ solutions. Radiochim. Acta 96 (9–11), 551–560. https://doi.org/10.1524/ract.2008.1536.

Rojo, H., Gaona, X., Rabung, T., Polly, R., García-Gutiérrez, M., Missana, T., Altmaier, M., 2021. Complexation of Nd(III)/Cm(III) with gluconate in alkaline NaCl and $CaCl_2$ solutions: solubility, TRLFS and DFT studies. Appl. Geochem. 126, 104864 https://doi.org/10.1016/j.apgeochem.2020.104864.

Schäfer, A., Horn, H., Ahlrichs, R., 1992. Fully optimized contracted Gaussian basis sets for atoms Li to Kr. J. Chem. Phys. 97 (4), 2571–2577. https://doi.org/10.1063/1.463096.

Schramke, J.A., Santillan, E.F.U., Peake, R.T., 2020. Plutonium oxidation states in the waste isolation Pilot plant repository. Appl. Geochem. 116, 104561 https://doi.org/10.1016/j.apgeochem.2020.104561.

Silva, A.M.N., Kong, X., Hider, R.C., 2009a. Determination of the pKa value of the hydroxyl group in the α-hydroxycarboxylates citrate, malate and lactate by 13C NMR: implications for metal coordination in biological systems. Biometals 22 (5), 771–778. https://doi.org/10.1007/s10534-009-9224-5.

Silva, A.M.N., Kong, X., Parkin, M.C., Cammack, R., Hider, R.C., 2009b. Iron(III) citrate speciation in aqueous solution. Dalton Trans. 40, 8616. https://doi.org/10.1039/b910970f.

Skerencak, A., Panak, P.J., Neck, V., Trumm, M., Schimmelpfennig, B., Lindqvist-Reis, P., Klenze, R., Fanghänel, T., 2010. Complexation of Cm(III) with fluoride in aqueous solution in the temperature range from 20 to 90 °C. A joint TRLFS and quantum chemical study. J. Phys. Chem. B 114 (47), 15626–15634. https://doi.org/10.1021/jp107794u.

Strouse, J., 1977. Carbon-13 NMR studies of ferrous citrates in acidic and alkaline solutions. Implications concerning the active site of aconitase. J. Am. Chem. Soc. 99 (2), 572–580. https://doi.org/10.1021/ja00444a042.

Szabo, P.G., Tasi, A.G., Gaona, X., Polly, R., Maier, A.C., Hedström, S., Altmaier, M., Geckeis, H., 2022. Solubility of Ca(ii), Ni(ii), Nd(iii) and Pu(iv) in the presence of proxy ligands for the degradation of polyacrylonitrile in cementitious systems. Dalton Trans. 51 (24), 9432–9444. https://doi.org/10.1039/D2DT01409B.

Tamain, C., Bonato, L., Aupiais, J., Dumas, T., Guillaumont, D., Barkleit, A., Berthon, C., Solari, P.L., Ikeda-Ohno, A., Guilbaud, P., Moisy, P., 2020. Role of the hydroxo group in the coordination of citric acid to trivalent americium. Eur. J. Inorg. Chem. 2020 (14), 1331–1344. https://doi.org/10.1002/ejic.202000124.

Tasi, A., Gaona, X., Fellhauer, D., Bottle, M., Rothe, J., Dardenne, K., Polly, R., Grivé, M., Colàs, E., Bruno, J., Kallstrom, K., Altmaier, M., Geckeis, H., 2018a. Thermodynamic description of the plutonium – α-d-Isosaccharinic acid system I_ solubility, complexation and redox behavior. Appl. Geochem. 98, 247–264.

Tasi, A., Gaona, X., Fellhauer, D., Böttle, M., Rothe, J., Dardenne, K., Polly, R., Grivé, M., Colàs, E., Bruno, J., Källstrom, K., Altmaier, M., Geckeis, H., 2018b. Thermodynamic description of the plutonium – α–d–Isosaccharinic acid system ii: formation of quaternary Ca(II)–Pu(IV)–OH–ISA complexes. Appl. Geochem. 98, 351–366. https://doi.org/10.1016/j.apgeochem.2018.06.014.

Treutler, O., Ahlrichs, R., 1995. Efficient molecular numerical integration schemes. J. Chem. Phys. 102 (1), 346–354. https://doi.org/10.1063/1.469408.

United States Department of Energy, 2014. Compliance Recertification Application. Appendix MgO-2014 Magnesium Oxide As an Engineered Barrier. United States Department of Energy.

Von Arnim, M., Ahlrichs, R., 1999. Geometry optimization in generalized natural internal coordinates. J. Chem. Phys. 111 (20), 9183–9190. https://doi.org/10.1063/1.479510.

Wimmer, H., Klenze, R., Kim, J.I., 1992. A study of hydrolysis reaction of curium(III) by time resolved laser fluorescence spectroscopy. Radiochim. Acta 56 (2), 79–84. https://doi.org/10.1524/ract.1992.56.2.79.